*Electromagnetics*, 20:257–268, 2000

0272-6343/00 $12.00 + .00

# Characteristic-Based Finite-Volume Time-Domain Method for Scattering by Coated Objects

DAN JIAO
JIAN-MING JIN

Center for Computational Electromagnetics
Department of Electrical and Computer Engineering
University of Illinois at Urbana-Champaign
Urbana, Illinois, USA

J. S. SHANG

Air Vehicles Directorate
Air Force Research Laboratory
Wright-Patterson Air Force Base, Ohio, USA

*The characteristic-based finite-volume time-domain method is applied to analyze the scattering from conducting objects coated with lossy dielectric materials. Based on the characteristic-based finite-volume scheme, two numerical strategies are developed to model the electromagnetic propagation across different dielectric media. One introduces a connecting boundary to separate the total-field region from the scattered-field region. The other employs the scattered field formulation throughout the computational domain. These two strategies are verified by numerical experiments to be basically equivalent. A numerical procedure compatible with the finite-volume scheme is developed to guarantee the continuity of the tangential electric and magnetic fields at the dielectric interface. Rigorous boundary conditions for all the field components are formulated on the surface of the perfect electric conducting (PEC) objects. The numerical accuracy of the proposed technique has been validated by comparison with theoretical results.*

## Introduction

The characteristic-based time-domain method, developed in the computational fluid dynamics community (CFD) for solving the Euler equations, has been applied to solve electromagnetic problems in recent years (Shang, 1995a, 1995b, 1996, 1999; Shang & Gaitonde, 1995a, 1995b; Shang & Robert, 1996; Shankar, Hall, & Mohammadian, 1989; Shankar, Mohammadian, & Hall, 1990). The basic approach of the characteristic-based method is to reduce the three-dimensional system of equations to an approximate Riemann problem in each spatial direction. The

Received 11 October 1999; accepted 7 January 2000.
Address correspondence to Jian-Ming Jin, Dept. of Electrical and Computer Engineering, University of Illinois, 1406 West Green St., Urbana, IL 61801-2991, USA. E-mail: j–jin1@uiuc.edu.

sequence of one-dimensional problems is then solved to obtain the solution to the original problem (Shang, 1995a). The basic algorithm can be implemented for either the finite-difference or the finite-volume procedure. The characteristic-based algorithm has several advantages over other time-domain methods. First, it can suppress reflected waves from the truncated outer boundary by simply interdicting the incoming propagation from the split flux vectors. Second, the governing equation can be easily cast into a body-oriented curvilinear coordinate system, which greatly facilitates the computation of electromagnetic fields around a complex scatterer. Third, the equations in flux vector form are split according to the sign of the eigenvalues, which enforces the directional propagation of information for wave motion and hence provides a more robust stability than a central differencing scheme. In addition, it can achieve a higher order accuracy easily by using a higher order interpolation or extrapolation technique to construct the flux vector at the cell vertexes or interfaces (Shang & Gaitonde, 1995a).

Because of the above advantages, several researchers have pioneered the application of this method to the analysis of electromagnetic scattering problems (Shang, 1995a, 1996, 1999; Shang & Gaitonde, 1995b). However, a survey of literature reveals that the present effort is focused on the scattering by perfect electric conducting (PEC) objects, and there is little application of this method to the scattering by objects coated with lossy dielectric materials. However, this analysis is of great importance to practical applications, especially the reduction of radar cross section (RCS) of low observable targets. Although the characteristic-based method allows the discontinuous data to be transmitted unaltered throughout the entire computational domain (Shang, 1995a), it encounters two difficulties when it deals with a dielectric interface. First, it exhibits a pronounced dissipation error after a long-time propagation (Shang & Robert, 1996). Second, since the six components of Maxwell's equations are placed at the same point, much effort is needed to enforce the boundary conditions at the dielectric interface.

To solve this problem, two methods are carefully constructed in this paper based on the finite-volume scheme. One introduces a connecting boundary to separate the total-field region from the scattered-field region, so that the boundary conditions can be easily implemented on the dielectric interface, although the scattered-field data has to be exchanged with the total-field data near the connecting boundary. The other method employs the scattered field formulation throughout the domain of interest, and hence the data exchange near the connecting boundary can be avoided. However, more attention needs to be paid to deal with the dielectric interface. Both of these two methods apply the scattered field at the truncated outer boundary, which enhances the performance of the compatibility condition. Numerical experiments indicate that these two methods are basically equivalent. In order to improve the accuracy of the characteristic-based algorithm, rigorous boundary conditions are derived for all the field components on PEC surfaces in the generalized curvilinear coordinate system. A numerical scheme to characterize the dielectric interface is developed to correctly simulate the wave propagation across different media. To demonstrate the validity of the proposed method, a conducting sphere coated with electric or magnetic lossy media is simulated. The sphere is considered due to the availability of the theoretical results. It is shown that the present method successfully captures the interaction of electromagnetic waves with the perfectly conducting surface and the dielectric interface.

## Formulation

In this section, the basic numerical scheme of the characteristic-based finite-volume method is described first. Two methods are then developed to analyze the scattering from coated objects. Finally, a detailed formulation is presented to characterize the PEC surface and the dielectric interface.

### *Governing Equations*

In a generalized curvilinear coordinate system $(\xi, \eta, \zeta)$, the governing equation for the total field in a homogeneous medium can be written as (Shang, 1995a)

$$\frac{\partial \mathbf{U}}{\partial t} + \frac{\partial \mathbf{F}}{\partial \xi} + \frac{\partial \mathbf{G}}{\partial \eta} + \frac{\partial \mathbf{H}}{\partial \zeta} = -\mathbf{J}. \tag{1}$$

The transformed dependent variables $\mathbf{U}$ and the flux vectors $\mathbf{F}, \mathbf{G}, \mathbf{H}$ in the above equation are given by

$$\begin{aligned} \mathbf{U} &= \overline{\mathbf{U}}/V, \quad \mathbf{J} = \overline{\mathbf{J}}/V, \\ \mathbf{F} &= \left(\xi_x \overline{\mathbf{F}} + \xi_y \overline{\mathbf{G}} + \xi_z \overline{\mathbf{H}}\right)/V, \\ \mathbf{G} &= \left(\eta_x \overline{\mathbf{F}} + \eta_y \overline{\mathbf{G}} + \eta_z \overline{\mathbf{H}}\right)/V, \\ \mathbf{H} &= \left(\zeta_x \overline{\mathbf{F}} + \zeta_y \overline{\mathbf{G}} + \zeta_z \overline{\mathbf{H}}\right)/V, \end{aligned} \tag{2}$$

where

$$\overline{\mathbf{U}} = \begin{Bmatrix} B_x \\ B_y \\ B_z \\ D_x \\ D_y \\ D_z \end{Bmatrix}, \tag{3}$$

$$\overline{\mathbf{F}} = \begin{Bmatrix} 0 \\ -D_z/\varepsilon \\ D_y/\varepsilon \\ 0 \\ B_z/\mu \\ -B_y/\mu \end{Bmatrix}, \quad \overline{\mathbf{G}} = \begin{Bmatrix} D_z/\varepsilon \\ 0 \\ -D_x/\varepsilon \\ -B_z/\mu \\ 0 \\ B_x/\mu \end{Bmatrix}, \quad \overline{\mathbf{H}} = \begin{Bmatrix} -D_y/\varepsilon \\ D_x/\varepsilon \\ 0 \\ B_y/\mu \\ -B_x/\mu \\ 0 \end{Bmatrix}. \tag{4}$$

Terms like $\xi_x$ are known as the metrics of the coordinate transformation and $V$ represents the Jacobian of the coordinate transformation. They are jointly determined by the nodes and edges of the elementary cell. Taking the lossy effect into

consideration, the right-hand side $\bar{\mathbf{J}}$ is expressed as

$$\bar{\mathbf{J}} = \begin{Bmatrix} \sigma_m B_x/\mu \\ \sigma_m B_y/\mu \\ \sigma_m B_z/\mu \\ \sigma_e D_x/\varepsilon + J_x \\ \sigma_e D_y/\varepsilon + J_y \\ \sigma_e D_z/\varepsilon + J_z \end{Bmatrix}. \tag{5}$$

Equation (1) can be integrated over an arbitrary volume $\Omega$ to obtain

$$\int\int\int_{\Omega} \mathbf{U}_t \, d\Omega + \int\int\int_{\Omega} (\mathbf{F}_\xi + \mathbf{G}_\eta + \mathbf{H}_\zeta) \, d\Omega = -\int\int\int_{\Omega} \mathbf{J} \, d\Omega, \tag{6}$$

which can be written as

$$\int\int\int_{\Omega} \mathbf{U}_t \, d\Omega + \int\int\int_{\Omega} (\nabla \cdot \mathbf{W}) \, d\Omega = -\int\int\int_{\Omega} \mathbf{J} \, d\Omega, \tag{7}$$

where

$$\mathbf{W} = \mathbf{F}\hat{\xi} + \mathbf{G}\hat{\eta} + \mathbf{H}\hat{\zeta}. \tag{8}$$

Application of the divergence theorem to the second integral in (7) gives

$$\int\int\int_{\Omega} \mathbf{U}_t \, d\Omega + \int\int_{S} (\mathbf{W} \cdot \hat{n}) \, dS = -\int\int\int_{\Omega} \mathbf{J} \, d\Omega, \tag{9}$$

in which $\hat{n}$ is the unit vector normal to the surface $S$ bounding the volume $\Omega$. The construction of the flux vectors $\mathbf{F}$, $\mathbf{G}$, and $\mathbf{H}$ at the interface of each cell adopts the concept of splitting introduced by Steger and Warming for CFD (Shang & Robert, 1996). If the cell-centered finite-volume scheme is employed, the flux vectors can be split as

$$\begin{aligned} \mathbf{F}_{i+\frac{1}{2}} &= \mathbf{A}^+ U_{i+\frac{1}{2}}^L + \mathbf{A}^- U_{i+\frac{1}{2}}^R, \\ \mathbf{G}_{j+\frac{1}{2}} &= \mathbf{B}^+ U_{j+\frac{1}{2}}^L + \mathbf{B}^- U_{j+\frac{1}{2}}^R, \\ \mathbf{H}_{k+\frac{1}{2}} &= \mathbf{C}^+ U_{k+\frac{1}{2}}^L + \mathbf{C}^- U_{k+\frac{1}{2}}^R, \end{aligned} \tag{10}$$

where the superscripts $L$ and $R$ denote the reconstructed dependent variables at the left and the right sides of a cell interface. Readers can refer to the literature (Shang & Robert, 1996) for the detailed formulation of the positive and negative coefficient matrices. The states $\mathbf{U}^L$ and $\mathbf{U}^R$ at any interface are constructed by a windward-biased formula:

$$\begin{aligned} U_{i+\frac{1}{2}}^L &= U_i + \frac{\phi}{4}[(1-k)(U_i - U_{i-1}) + (1+k)(U_{i+1} - U_i)], \\ U_{i+\frac{1}{2}}^R &= U_{i+1} - \frac{\phi}{4}[(1+k)(U_{i+1} - U_i) + (1-k)(U_{i+2} - U_{i+1})]. \end{aligned} \tag{11}$$

If $k = \frac{1}{3}$ and $\phi = 1$, the algorithm is spatially third-order accurate. The fractional-step method (Shang, 1995b) or the Runge–Kutta family of single-step multistage procedures (Shang, 1995a, 1999) can be employed to accomplish the time integration. In this paper, a single-step two-stage Runge–Kutta scheme is used to guarantee the second-order accuracy.

When the characteristic-based finite-volume algorithm is used to analyze a coated scatterer, a connecting boundary can be introduced to separate the total-field region from the scattered-field region. The introduction of the connecting boundary provides two advantages. First, the boundary condition at the dielectric interface can be more easily satisfied by the formulation of the total field. Second, the application of the scattered field at the outer boundary of the computational domain enhances the performance of the compatibility condition.

Since a connecting boundary is introduced to the finite-volume scheme, (11) needs to be modified near the connecting boundary. Referring to Figure 1 which portrays a row of finite-volume cells with the face $i + \frac{1}{2}$ separating the total-field and the scattered-field regions, the construction of the states at the cell face $i + \frac{1}{2}$, $(i - 1) + \frac{1}{2}$, and $(i + 1) + \frac{1}{2}$ should be adjusted. As an example, the modified formulation of the total field $\mathbf{U}_{i+\frac{1}{2}}$ is given as follows:

$$U_{i+\frac{1}{2}}^{L} = U_i + \frac{\phi}{4}\left[(1-k)(U_i - U_{i-1}) + (1+k)(U_{i+1} + U_{i+1}^{inc} - U_i)\right],$$

$$U_{i+\frac{1}{2}}^{R} = U_{i+1} + U_{i+1}^{inc} - \frac{\phi}{4}\left[(1+k)(U_{i+1} + U_{i+1}^{inc} - U_i)\right.$$

$$\left.+(1-k)(U_{i+2} + U_{i+2}^{inc} - U_{i+1} - U_{i+1}^{inc})\right]. \qquad (12)$$

Another strategy for the analysis of a coated scatterer is to use the scattered field formulation throughout the computational domain. From Maxwell's equa-

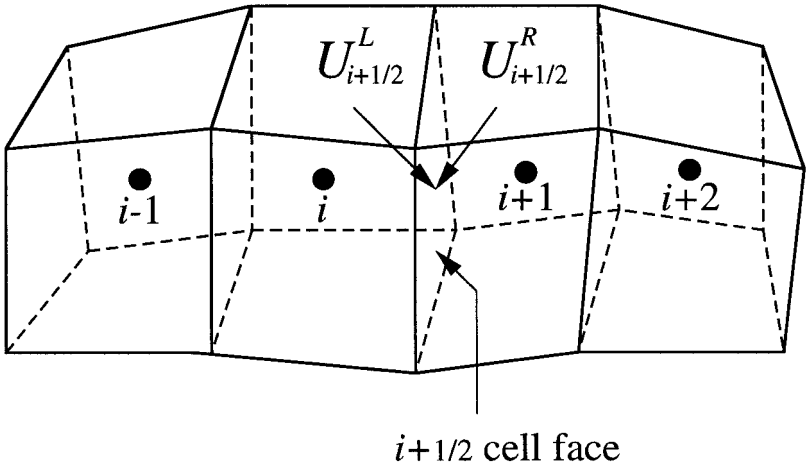


**Figure 1.** Geometry of a row of finite-volume cells.

tions, it can be easily derived that the scattered field satisfies

$$\frac{\partial \mathbf{U}_s}{\partial t} + \frac{\partial \mathbf{F}_s}{\partial \xi} + \frac{\partial \mathbf{G}_s}{\partial \eta} + \frac{\partial \mathbf{H}_s}{\partial \zeta} = -\begin{Bmatrix} \mathbf{J}_m \\ \mathbf{J}_e \end{Bmatrix}, \tag{13}$$

where

$$\mathbf{J}_m = \nabla \times \frac{\mathbf{D}^{inc}}{\varepsilon} + \frac{\partial \mathbf{B}^{inc}}{\partial t},$$

$$\mathbf{J}_e = -\nabla \times \frac{\mathbf{B}^{inc}}{\mu} + \frac{\partial \mathbf{D}^{inc}}{\partial t}. \tag{14}$$

Obviously, $\mathbf{J}_m$ and $\mathbf{J}_e$ are nonzero only within the coating layers. In (13), the dependent variable $\mathbf{U}_s$ is made up of the scattered-field components. The flux vectors $\mathbf{F}_s$, $\mathbf{G}_s$, and $\mathbf{H}_s$ take the same form as (2) except that they are determined by the scattered field. When the lossy phenomenon is considered, the right-hand side of equation (13) is correspondingly modified to

$$\mathbf{J}_m = \nabla \times \frac{\mathbf{D}^{inc}}{\varepsilon} + \frac{\partial \mathbf{B}^{inc}}{\partial t} + \sigma_m \frac{\mathbf{B}}{\mu},$$

$$\mathbf{J}_e = -\nabla \times \frac{\mathbf{B}^{inc}}{\mu} + \frac{\partial \mathbf{D}^{inc}}{\partial t} + \sigma_e \frac{D}{\varepsilon}, \tag{15}$$

where **B** and **D** are the total field components. At the dielectric interface as well as the scatterer surface, the incident field should be added to the scattered field to enforce the boundary condition. Since the two strategies basically produce the same result, the first one, which employs a connecting boundary, is used to generate numerical examples in this paper.

### *Boundary Condition Implementation*

The correct implementation of boundary conditions is of great importance to the accuracy of the numerical procedure. It follows naturally from the fact that when the governing equations are identical, only the different boundary conditions generate different solutions.

For the analysis of conducting objects coated with dielectric materials, there are three kinds of boundary conditions involved. One is the PEC boundary, another is the dielectric interface, the third is the outer boundary where the wave exits.

On the surface of the perfect electric conductors, in addition to the well-known boundary conditions

$$E_\eta = E_\zeta = H_\xi = 0, \tag{16}$$

the following boundary conditions can be derived from Maxwell's equations in a generalized orthogonal curvilinear coordinate system

$$\frac{\partial(h_\eta h_\zeta E_\xi)}{\partial \xi} = 0,$$

$$\frac{\partial(h_\eta H_\eta)}{\partial \xi} = 0,$$

$$\frac{\partial(h_\zeta H_\zeta)}{\partial \xi} = 0, \tag{17}$$

where $\eta$ and $\zeta$ are along the direction tangential to the PEC surface, whereas $\xi$ points to the normal direction outside the PEC conductor and $h_\eta = |\nabla\eta|^{-1}$ and $h_\zeta = |\nabla\zeta|^{-1}$ are the scale factors along the $\eta$ and $\zeta$ directions, respectively. Here, $E_\xi$, $H_\eta$, and $H_\zeta$ denote the total field components. If the scattered field formulation is used, the incident field should be taken into account to implement the PEC boundary condition. Since the dependent variables are expressed in the Cartesian coordinate system, a coordinate transformation needs to be applied to carry out the boundary condition implementation.

At the dielectric interface, (11) should be modified to guarantee the continuity of the tangential electric and magnetic fields. Referring to Figure 1, assume that the cell face $i + \frac{1}{2}$ denotes the dielectric interface; the following steps can be taken to implement the boundary conditions.

- *Step 1*: Transform the dependent variables $\mathbf{U}$ at cell centers $i-1, i, i+1$, and $i+2$ to $\mathbf{U}_{t,\hat{\imath}}$ which is made up of $B_I, B_J, B_K, D_I, D_J$, and $D_K$, where the unit vectors $\hat{I}, \hat{J}$, and $\hat{K}$ construct a locally orthogonal coordinate system in which $\hat{I}$ is normal to the cell interface while $\hat{J}$ and $\hat{K}$ lie on the interface.
- *Step 2*: Construct $\mathbf{U}^L_{t,i+1/2}$ and $\mathbf{U}^R_{t,i+1/2}$ at the dielectric interface according to the following formulation.

  For $B_J$ and $B_K$:

$$U^L_{t,i+\frac{1}{2}} = \frac{1}{2}U_{t,i}(\mu_l + \mu_r)/\mu_l + \frac{\phi}{8}$$
$$\times\{(1-k)[U_{t,i}(\mu_l + \mu_r)/\mu_l - U_{t,i-1}(\mu_l + \mu_r)/\mu_l]$$
$$+(1+k)[U_{t,i+1}(\mu_l + \mu_r)/\mu_r - U_{t,i}(\mu_l + \mu_r)/\mu_l]\}$$

  For $D_J$ and $D_K$:

$$U^L_{t,i+\frac{1}{2}} = \frac{1}{2}U_{t,i}(\varepsilon_l + \varepsilon_r)/\varepsilon_l + \frac{\phi}{8}$$
$$\times\{(1-k)[U_{t,i}(\varepsilon_l + \varepsilon_r)/\varepsilon_l - U_{t,i-1}(\varepsilon_l + \varepsilon_r)/\varepsilon_l]$$
$$+(1+k)[U_{t,i+1}(\varepsilon_l + \varepsilon_r)/\varepsilon_r - U_{t,i}(\varepsilon_l + \varepsilon_r)/\varepsilon_l]\}$$

7
For $B_I$ and $D_I$:

$$U^L_{t,i+\frac{1}{2}} = U_{t,i} + \frac{\phi}{4}[(1-k)(U_{t,i} - U_{t,i-1}) + (1+k)(U_{t,i+1} - U_{t,i})], \quad (18)$$

where the subscripts $l$ and $r$ denote the left and right sides of the dielectric interface. The transformed dependent variables at the right side of the dielectric interface, $\mathbf{U}^R_{t,i+1/2}$, can be constructed based on the same principle.

- *Step 3*: Recover $\mathbf{U}^L_{i+1/2}$ and $\mathbf{U}^R_{i+1/2}$, which is made up of $B_x, B_y, B_z, D_x, D_y$, and $D_z$, from $\mathbf{U}^L_{t,i+1/2}$ and $\mathbf{U}^R_{t,i+1/2}$ constructed in the locally orthogonal coordinate system $\{\hat{I}, \hat{J}, \hat{K}\}$.

The compatibility condition at the outer boundary can be easily accomplished by setting the incoming fluxes to be zero (Shang, 1995a). If one of the transformed coordinates is aligned with the direction of wave propagation, the exact no-reflection condition can be achieved.

## Numerical Examples

The numerical procedure described above has been implemented. In this section, several examples are considered here for validation purposes.

The first example is a coated conducting sphere with a radius of one free-space wavelength. The relative permittivity of the coating is 2.56. The thickness is $1/30$ dielectric wavelength. The connecting boundary is placed at two grids away from the coating surface. The outer boundary is placed at three wavelengths away. Including the discretization within the coating, in total 41 grids are used along the radial direction, generated by hyperbolic stretching. The surface density is chosen to be 25 grids per wavelength. The Stratton–Chu formulation (see Crispin & Seigel, 1968) is employed for the transformation from the near field to the far field. Figure 2 shows the calculated bistatic RCS of the sphere under the H-polarized plane wave incidence. It agrees well with the solution from the Mie series. Next, the lossy effect of the dielectric medium is considered. In this case, the relative permittivity becomes a complex number, which is assumed to be $2.56 - j4.0$, indicating the conductivity to be $4\omega\varepsilon_0$, where $\omega$ is the angular frequency. From Figure 3, it can be seen clearly that the present scheme captures the lossy phenomenon successfully. In order to make the validation more persuasive, next we double the coating thickness to $1/15$ dielectric wavelength. The complex permittivity is still assumed to be $2.56 - j4.0$. Figure 4 gives the resultant bistatic RCS. Obviously, it agrees very well with the Mie series.

The second example is a conducting sphere coated with a magnetic material. The coating layer is $1/30$ dielectric wavelength thick with a relative permeability 2.3. For lossy coating, the complex permeability is chosen to be $2.3 - j4.0$. Figure 5 shows the calculated bistatic RCS with and without loss under the H-polarized plane wave incidence. It is evident that the numerical results agree very well with the Mie series. Note that the lossy and lossless cases differ greatly from each other. Figure 6 gives the V-polarized bistatic RCS. Similarly, the agreement between the numerical and the theoretical results is satisfactory.

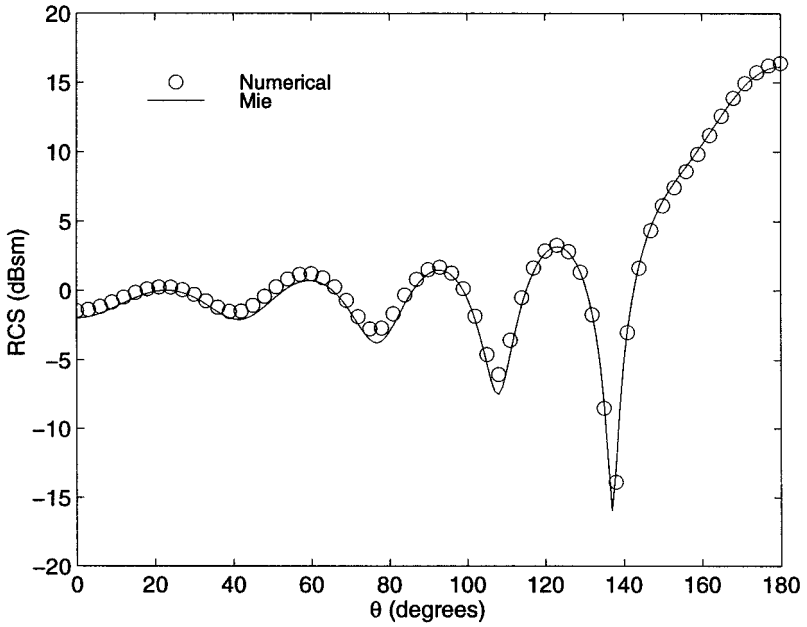


**Figure 2.** Bistatic RCS of a conducting sphere coated with a lossless dielectric medium, $R = \lambda_0$, $\varepsilon_r = 2.56$, dielectric thickness $= \lambda/30$.

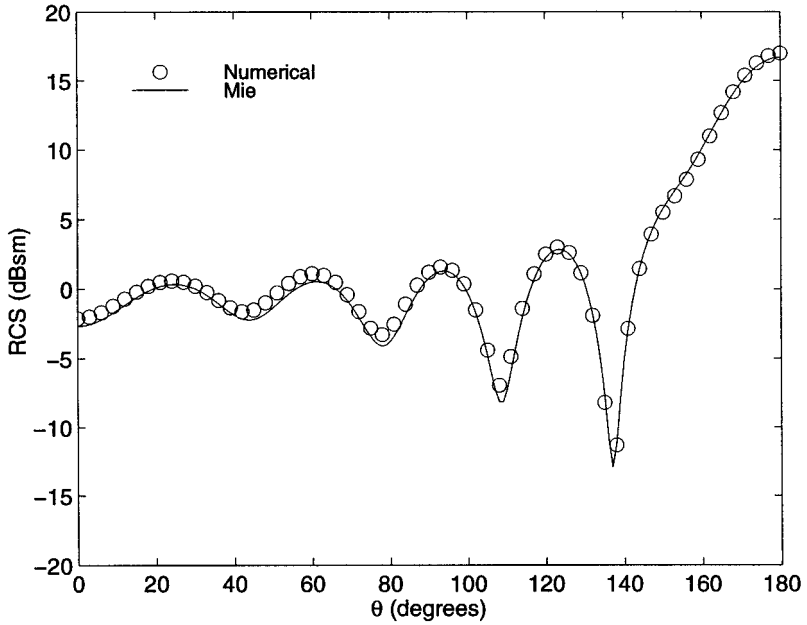


**Figure 3.** Bistatic RCS of a conducting sphere coated with a lossy dielectric medium, $R = \lambda_0$, $\varepsilon_r = 2.56 - j4$, dielectric thickness $= \lambda/30$.

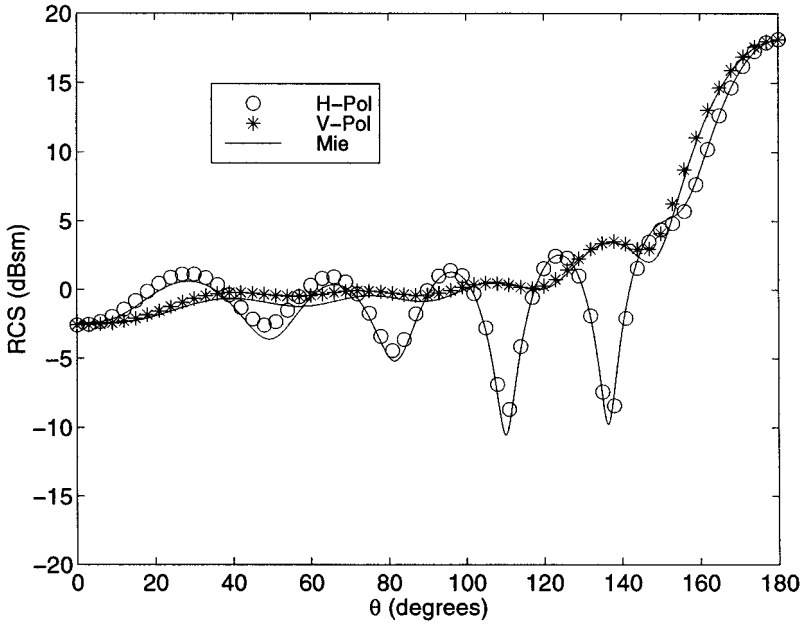


**Figure 4.** Bistatic RCS of a conducting sphere coated with a lossy dielectric medium, $R = \lambda_0$, $\varepsilon_r = 2.56 - j4$, dielectric thickness $= \lambda/15$.

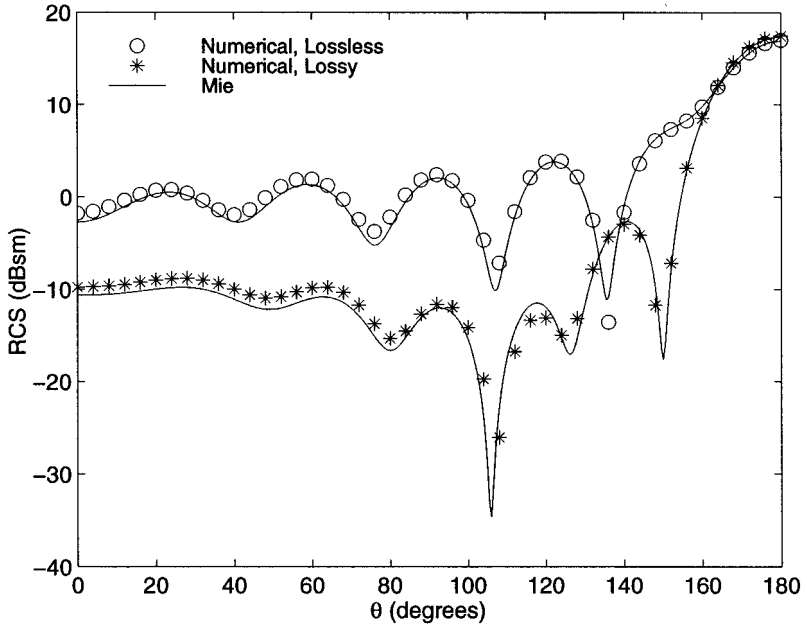


**Figure 5.** Bistatic RCS of a conducting sphere coated with a magnetic dielectric medium, $R = \lambda_0$, dielectric thickness $= \lambda/30$, HH-polarization, $\mu_r = 2.3$ for lossless coating, $\mu_r = 2.3 - j4$ for lossy coating.

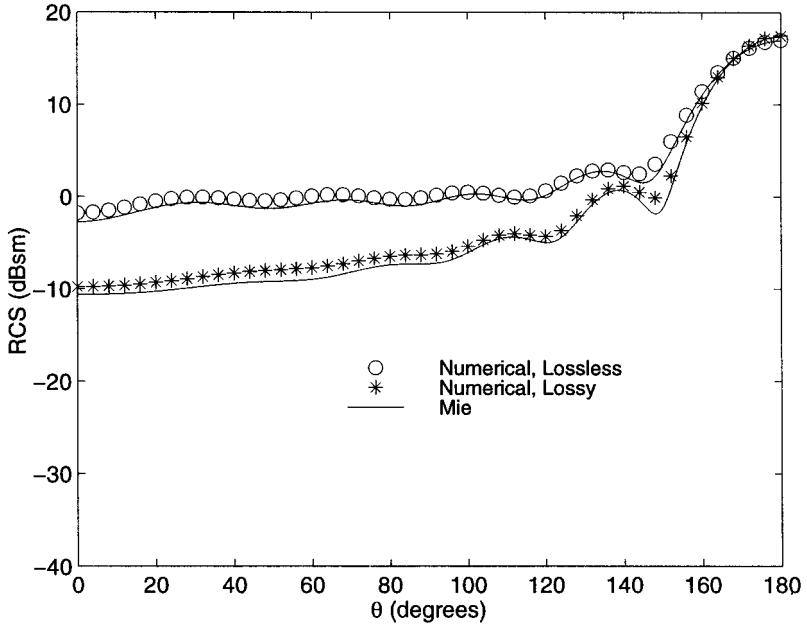


**Figure 6.** Bistatic RCS of a conducting sphere coated with a magnetic medium, $R = \lambda_0$, dielectric thickness $= \lambda/30$, VV-polarization, $\mu_r = 2.3$ for lossless coating, $\mu_r = 2.3 - j4$ for lossy coating.

## Conclusion

In this paper, the characteristic-based finite-volume method is extended to the analysis of scattering from conducting objects coated with lossy dielectric materials. A numerical scheme is presented to enforce the boundary conditions at the dielectric interface. Rigorous boundary conditions on the surface of perfect conductors are developed to improve the accuracy of the numerical procedure. Numerical results are presented to validate the proposed method.

## References

Crispin, J. W., & K. M. Seigel, eds. 1968. *Methods of radar cross-section analysis*. New York: Academic Press, pp. 3–32.

Shang, J. S. 1995a. Characteristic-based algorithms for solving the Maxwell equations in the time domain. *IEEE Antennas and Propagation Magazine* 37:15–25.

Shang, J. S. 1995b. A fractional-step method for solving 3D, time-domain Maxwell equations. *Journal of Computational Physics* 118:109–119.

Shang, J. S. 1996. Time-domain electromagnetic scattering simulations on multicomputers. *Journal of Computational Physics* 128:381–390.

Shang, J. S. 1999. High-order compact-difference schemes for time-dependent Maxwell equations. *Journal of Computational Physics* 153:312–333.

Shang, J. S., & D. Gaitonde. 1995a. Characteristic-based, time-dependent Maxwell equations solvers on a general curvilinear frame. *AIAA Journal* 33(3):491–498.

Shang, J. S., & D. Gaitonde. 1995b. Scattered electromagnetic field of a reentry vehicle. *AIAA J. Spacecraft and Rockets* 32(2):294–301.

Shang, J. S., & M. F. Robert. 1996. A comparative study of characteristic-based algorithms for the Maxwell equations. *Journal of Computational Physics* 125:378–394.

Shankar, V., W. Hall, & A. H. Mohammadian. 1989. A three-dimensional Maxwell's equation solver for computation of scattering from layered media. *IEEE Trans. Magn.* 25(4):3098–3103.

Shankar, V., A. H. Mohammadian, & W. Hall. 1990. A time-domain, finite-volume treatment for the Maxwell equations. *Electromagnetics* 10:127–145.